

Large dilatational hyperelasticity of glasses en route to cavitation failure

Pawandeep Kaur^{1,*}, Noam Ottolenghi^{1,*}, Edan Lerner², David Richard^{3,†} and Eran Bouchbinder^{1,‡}

¹*Chemical and Biological Physics Department, Weizmann Institute of Science, Rehovot 7610001, Israel*

²*Institute for Theoretical Physics, University of Amsterdam,
Science Park 904, 1098 XH Amsterdam, The Netherlands*

³*PMMH, CNRS, ESPCI Paris, Université PSL, Sorbonne Université, Université Paris Cité, France*

Materials deform elasto-plastically and fail under various loading conditions, typically quantified by the stress triaxiality, which is the ratio between the dilatational (hydrostatic) stress and the deviatoric (shear-like) one. We show that the elasto-plastic deformation of glasses approaching failure qualitatively differ for large and small stress triaxiality levels. Specifically, in the former limit, glasses reveal a strong hyperelastic (nonlinear elastic) response with minute plasticity, largely independently of the quenching rate across the glass transition. Yet, glassy disorder gives rise to significant elastic (reversible) nonaffine deformation, accompanied by the formation of micro-cavities. A small fraction of the latter is irreversible, i.e., survives unloading prior to the onset of failure, and may serve as nucleation sites for failure in the form of large-scale cavitation, upon which the glass loses a significant fraction of its load-bearing capacity. These results are contrasted with glass behavior in the limit of vanishing stress triaxiality and their universality across different glass formers is demonstrated. Finally, the implications of our findings for understanding glass deformation and failure under realistic stress conditions are discussed.

I. Introduction

The ways materials deform and fail depend not only on the magnitude of the force applied to them, but also on its symmetry, i.e., on the tensorial nature of the material stress state. The latter is commonly quantified by the stress triaxiality [1], which measures the relative magnitude of the hydrostatic (dilatational, volumetric) and deviatoric (shear-like, volume-preserving) stress. While the effect of stress triaxiality on the elasto-plastic deformation and failure modes of crystalline, polycrystalline and porous ductile solids has been extensively studied [2–18], characterizing and understanding the corresponding physical effects in non-crystalline, glassy/amorphous solids lag behind (though, note [19–22], for example).

Much effort has been devoted to studying the micromechanics and statistical-mechanical properties of deforming glasses in the limit of vanishing stress triaxiality, i.e., under predominantly shear loading. Realistic failure, however, typically takes place under significantly different physical conditions. For example, the stress state ahead of the tip of a quasi-static crack defect in quasi-two-dimensional systems is purely hydrostatic [23, 24] and high stress triaxiality levels emerge in various three-dimensional loading configurations [25–31]. Elevated stress triaxiality is indicated by the formation of micro-cavities near the crack tip [32–37], as well as by the appearance of dimpled features in the fractography of ductile Bulk Metallic Glasses [38, 39].

Preliminary steps in closing the aforementioned gap have been recently made [20, 40, 41]. Specifically, some

similarities between the low-temperature elementary processes that mediate structural rearrangements in glasses under large and small stress triaxiality levels have been demonstrated [40–42]. Earlier work established that under shear loading, structural rearrangements in glasses correspond to saddle-node bifurcations (instabilities) in the potential energy landscape, whose complexity reflects the disordered nature of glasses, formed by quenching liquids through the glass transition. These instabilities, termed shear transformations, are localized in space and are the main carriers of plastic deformation in glasses under shear [43, 44], playing analogous roles to mobile dislocations in crystalline solids [45]. It has been recently shown that the very same instabilities occur under large stress triaxiality levels (predominantly dilatational deformation), where the symmetry of the loading quantitatively affects the geometry of the unstable modes [41].

Here, we show that in fact the elasto-plastic deformation of glasses approaching failure qualitatively differ for large and small stress triaxiality levels. By employing large-scale computer simulations and an array of theoretical and computational tools, we show that under large stress triaxiality, glasses reveal a strong hyperelastic (nonlinear elastic) response with minute plasticity, largely independently of the quench rate through the glass transition, which strongly affects the state of glassy disorder/stability. Consequently, dilatational elastic softening is accounted for by a first-principles zero-strain nonlinear elastic expansion, which is terminated by a large-scale cavitation instability.

The dilatational deformation includes a significant nonaffine component — a manifestation of the intrinsically disordered nature of glasses —, which is predominantly reversible and accompanied by the formation of micro-cavities. A small fraction of the latter is irreversible, i.e., survives unloading prior to the onset of aforementioned large-scale cavitation, and may serve as

* Contributed equally

† david.richard@espci.fr

‡ eran.bouchbinder@weizmann.ac.il

nucleation sites for the latter, upon which the glass loses a significant fraction of its load-bearing capacity. These results are contrasted with the corresponding behavior of sheared glasses. The generality of our findings, which have important implications for understanding the deformation and failure dynamics of glasses under realistic stress conditions, is demonstrated across various classes of computer glasses.

II. Macroscopic shear and dilatational glassy response

Obtaining fundamental insight into glassy deformation requires access to small lengthscales that are currently out of reach experimentally. We consequently resort to computer simulations that open a unique window to such scales, yet allowing to simulate rather large systems and to extract macroscopic response quantities. We first study a polydisperse, Lennard-Jones-type (LJ) computer glass [46], whose main advantage is that it allows to obtain glasses that span a wide range of thermal annealing states (quench rates) upon glass formation, including deeply annealed states that feature glass disorder/stability comparable to laboratory glasses [47]. All the glass samples we consider feature a vanishingly small initial pressure, representing realistic ambient conditions.

We also employ an athermal quasistatic (AQS) deformation procedure that mimics the limit of low temperatures and strain rates [48]. Its main advantage is that it allows to disentangle the effects of thermal fluctuations and finite deformation rates from the dominant effect of glassy disorder on the deformation, and to obtain — both theoretically and numerically — quantitative information about various physical observables. The details of the computer model, glass formation procedure and loading protocols are provided in the Methods and *SI Appendix*.

We subject the very same glasses to both shear (vanishing stress triaxiality), quantified by a shear strain parameter γ , and hydrostatic tension/dilation (arbitrarily large stress triaxiality), quantified by a dilatational strain parameter ϵ , and focus first on global quantities. We employ computer glasses composed of $N = 10^4 - 10^6$ atoms/particles, depending on the question posed and computational feasibility. In Fig. 1a, we present normalized stress-strain curves for a quickly quenched glass (i.e., a poorly annealed one, resulting in a highly disordered state) under shear (brown) and dilation (green). Here, and throughout the paper, we use the zero-strain shear (bulk) modulus μ_0 (K_0) to normalize the shear stress (hydrostatic tension).

A clear signature of the highly disordered state of the glass sample used is the lack of a distinct yielding transition under shear, i.e., it features a continuous crossover from a linear elastic regime at small γ to steady flow at large γ (saturating at a flow stress of $\sigma/\mu_0 \simeq 0.05$, see *SI Appendix*), with no shear-banding. This is in sharp con-

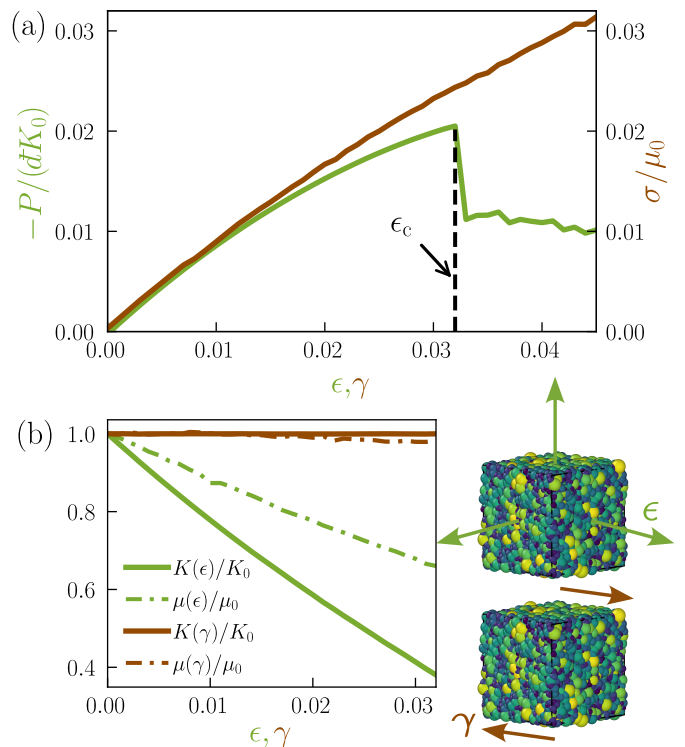


FIG. 1. (a) Stress-strain curves of the same glass sample ($N = 10^6$ particles) under dilation (green, left y -axis) and shear (brown, right y -axis), see also visual inset in panel (b). The hydrostatic pressure $-P$ (shear stress σ) is plotted against the dilatational (shear) strain parameter ϵ (γ), both normalized such that the dimensionless zero-strain modulus equals unity, where K_0 (μ_0) is the bulk (shear) modulus and d is space dimensionality (here $d = 3$). ϵ_c corresponds to the large-scale cavitation strain under dilation (see Fig. 6). See *SI Appendix* for details and definitions. (b) The corresponding strain-dependent bulk and shear moduli (up to the value of ϵ_c), see legend.

trast to the corresponding behavior under dilation, which reveals a stronger softening response and a sharp stress drop, corresponding to a large-scale cavitation instability, followed by continuous softening (for the response at yet larger dilatational strains, see *SI Appendix*). We hereafter denote the large-scale cavitation strain by ϵ_c and focus on strains smaller or equal to it. Our major goal is to elucidate the origin and physical significance of this difference.

To start characterizing the glass states along the stress-strain loading curve shown in Fig. 1a, we present in Fig. 1b the evolution of the *strain-dependent linear elastic constants* μ and K as a function of ϵ and γ (up to a value corresponding to ϵ_c), computed from analytic expressions (see *SI Appendix*). These should be distinguished from the tangent moduli (that correspond to the local derivatives of each stress with respect to the relevant strain parameter, see *SI Appendix*).

The results reveal sharp differences between shear

and dilation; while the linear elastic moduli are essentially independent of γ under shear, the corresponding quantities feature significant softening under dilation, where the bulk modulus $K(\epsilon)$ softens by $\sim 60\%$ as ϵ_c is approached and the shear modulus $\mu(\epsilon)$ by about half of it. The results in Fig. 1 may suggest that on the one hand, the dilatational response is “more brittle” (likewise, the shear response is “more ductile”) as it is accompanied by an abrupt and significant stress drop, but at the same time it is also “less brittle” as the stress drop is preceded by significant softening.

III. Microscopic measures of nonaffinity and structural rearrangements

To shed additional light on these somewhat conflicting interpretations, we next consider microscopic observables related to the disordered nature of glasses and their structural evolution under deformation. A distinguishing feature of glassy disorder is nonaffine deformation, i.e., a local deformation that does not follow the globally applied deformation due to disorder-induced mismatch forces [49, 50]. We construct a dimensionless measure of nonaffinity denoted as $\eta_{n.a.}$, which quantifies the fraction of the deformation that cannot be accounted for by a local affine deformation, allowing to compare on equal footing nonaffinity under shear and dilation, see *SI Appendix*. In Fig. 2a, we plot $\eta_{n.a.}$ for a sheared and dilated glass. It is observed that the overall nonaffinity is significantly larger under shear.

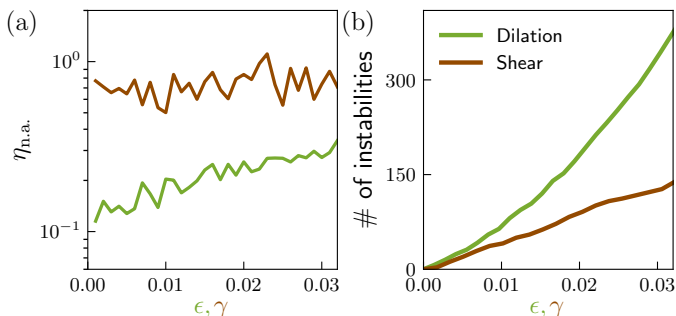


FIG. 2. (a) The dimensionless measure of nonaffine deformation $\eta_{n.a.}$ vs. strain under both dilation and shear (as in Fig. 1 but with $N=10^5$), see text for details and discussion. (b) The corresponding accumulated number of structural rearrangements (instabilities).

In many cases, nonaffinity is related to the structural evolution of the glass due to configurational rearrangements. Therefore, we take advantage of the employed AQS deformation, which allows to exhaustively identify all structural rearrangement/instability events, each one corresponding to a single saddle-node bifurcation. We enumerate all instabilities under shear and dilation, and present in Fig. 2b their accumulated number as a function

of strain. It is observed that the rate (per unit strain) of structural rearrangements is larger under dilation (by a factor somewhat larger than two).

It is thus tempting to hypothesize that the increased rate of structural rearrangements might explain the dramatic excess of softening under dilation observed in Fig. 1b. Yet, the nature of the structural rearrangements and their magnitude, not just their rate, can play important roles as well. Taken together, the results presented in Fig. 2 do not offer a conclusive physical explanation for the fundamental differences between the glass response to shear and dilation observed in Fig. 1.

IV. Macroscopic reversibility and irreversibility revealed by unloading

The above results showed that nonaffinity and structural rearrangements, which are generic features of glassy deformation, are present under both shear and dilation, in line with recent findings [40, 41], yet the emerging quantitative differences appear to fall short of accounting for the qualitative differences observed in Fig. 1. What is missing is a deeper understanding of which of (or the degree to which) the aforementioned deformation processes are reversible or irreversible. Put differently, we need to identify the elastic and plastic components of the deformation under the different stress triaxiality levels. The most definitive way to achieve this is by unloading the glass from different loading levels, as done in Figs. 3a-b.

The results reveal striking differences between shear and dilation. Figure 3a shows that unloading dilatational states with $\epsilon < \epsilon_c$ leads to a recovery of the macroscopic initial state, with no significant hysteresis and residual plastic strain. It indicates that minute dissipation is involved in the loading process up to ϵ_c , i.e., that the corresponding deformation is predominantly elastic/reversible. This means that the dilatational softening observed in Fig. 1b mainly corresponds to hyperelasticity, i.e., to nonlinear elasticity, not to plasticity. Likewise, the dilatational nonaffinity of Fig. 2a is expected to be predominantly elastic and the corresponding structural rearrangements quantified in Fig. 2b to be small and/or reversible upon unloading. Significant hysteresis and residual plastic strains emerge only after the large stress drop occurring at ϵ_c , as shown in Fig. 3a.

The situation is markedly and qualitatively different when the very same glass is unloaded after being sheared, as shown in Fig. 3b. As expected from a continuous elasto-plastic yielding transition, the unloading curves observed in Fig. 3b feature a slope approximately corresponding to μ_0 , and reveal large hysteresis and residual plastic strains. These are consistent with the absence of elastic softening under shear, as observed in Fig. 1b, and show that the shear nonaffinity of Fig. 2a is predominantly plastic and that the corresponding structural rearrangements quantified in Fig. 2b are predominantly

irreversible plastic events.

Taken together, the results in Fig. 3 explain the origin of the fundamental shear/dilation differences of Fig. 1, and shed basic light on the findings of Fig. 2. The crux of the differences is that under shear, glass deformation is strongly plastic/irreversible, while under dilation it is predominantly elastic/reversible, revealing large hyperelasticity.

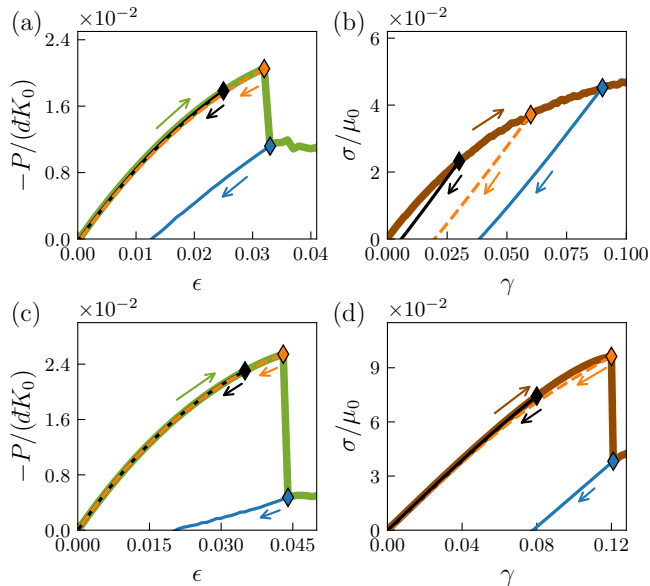


FIG. 3. (a-b) The same as Fig. 1a, but with unloading to zero strain added (the unloading points are marked by diamonds and guiding arrows are added). (c-d) The same as panels (a-b), but for a deeply annealed (slowly quenched) glass sample. See text for discussion.

V. Nonequilibrium thermal history effects

The structural rearrangements quantified in Fig. 2b do not give rise to significant plastic dissipation and stress relaxation. This implies that they are either small in magnitude or reversible upon unloading or both. Reversible structural rearrangements, i.e., saddle-node bifurcations that are elastically generated during loading, are documented for well annealed glasses deformed under shear [51–54]. We are therefore interested in exploring the differences in the deformation and failure modes of glasses under vastly different stress triaxiality levels also as a function of the glass thermal history.

The glass state analyzed in Fig. 3a-b was generated through a quick quench, leading to a large degree of disorder. We control the degree of annealing of a glass as it forms, i.e., its effective quench rate, through the ‘parent temperature’ T_p from which the equilibrium supercooled liquid is instantaneously brought into a zero-temperature inherent structure [55]. The employed computer glass can be very deeply annealed, leading to very stable glass

states [47, 56, 57].

In Fig. 3c-d, we present loading-unloading curves as in Fig. 3a-b, but for a much deeper supercooled glass state. The response to dilatational deformation, shown in Fig. 3c, is qualitatively similar to the corresponding dilatational response in Fig. 3a for a significantly less annealed glass, where the main quantitative difference is the much larger stress drop in the former. The response to shear deformation in Fig. 3d, however, is dramatically different from the corresponding shear response in Fig. 3b for a significantly less annealed glass. Notably, the loading-unloading curves in Fig. 3d (observed earlier, e.g., in [52, 53]) are qualitatively similar to the dilatational response in Fig. 3a,c, revealing no macroscopic residual plastic strain prior to the large stress drop.

These results point to yet another major difference between the shear and dilatational response of glasses, indicating that while the dilatational response is predominantly elastic prior to large-scale cavitation, largely independently of the glassy state of disorder (degree of thermal annealing), the macroscopic reversibility-irreversibility properties of the shear response strongly depend on it. The shear and dilatational response in Fig. 3c-d differ in two additional important respects: first, the physical (and spatial) origin of the large stress drops observed in the two cases is markedly different, i.e., it is large-scale cavitation under dilation (see Fig. 6a and *SI Appendix*), while it is large-scale shear-banding under shear [58–60]. Second, nonlinear elasticity is very small prior to shear-banding is very small, while it is very large under dilation, i.e., K can soften up to 75% over a dilatational strain of 3–4% (see *SI Appendix*, where the deeply annealed counterpart plot of Fig. 1b is presented).

VI. Microscopic irreversibility

In Fig. 3, we focused on macroscopic reversibility/irreversibility. Yet, it was also established above that microscopic glass deformation is accompanied by non-affinity and structural rearrangements, which can be either irreversible — and of variable magnitude — or reversible. Our goal here is to gain insight into *microscopic* reversibility/irreversibility at the level of individual structural rearrangements as a function of both stress triaxiality and the glass thermal history. In Fig. 4a, we illustrate the stress-strain portrait of both reversible and irreversible structural rearrangements/instabilities (‘events’).

Performing a microscopic reversibility/irreversibility analysis for individual structural instabilities over large strain intervals and system sizes is a daunting computational task. We therefore performed the analysis on the first instability in $N = 10^4$ glass samples generated under the same widely different thermal histories considered in Fig. 3, quantified by T_p , and deformed under dilation and shear (loading to the first instability and

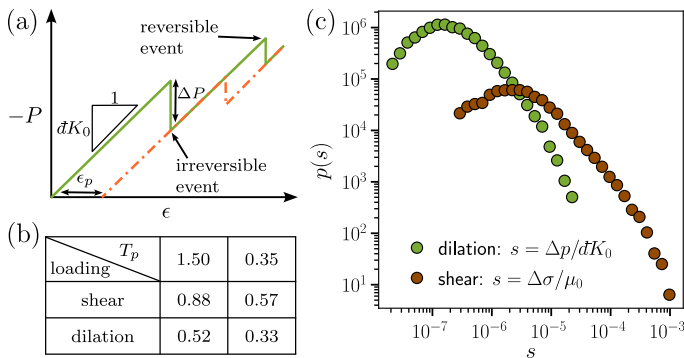


FIG. 4. (a) A stress-strain curve sketch, showing a loading portion (solid green line) followed by unloading (dashed-dotted orange line). It features a reversible structural rearrangement (event) and an irreversible one, resulting in a residual plastic strain ϵ_p . The sketch refers to dilation such that the slope corresponds to dK_0 (see Fig. 1a) and the irreversible stress drop to ΔP . (b) A table showing the fraction of irreversible events among the population of the first structural rearrangements in two glass ensembles of $M=100$ samples each and $N=10^4$, corresponding to high/low T_p values (horizontal direction) and loaded in shear/dilation (vertical direction). See text for discussion. (c) The distribution of dimensionless stress drops s under both dilation and shear (see legend), obtained for $M=100$ high T_p and $N=10^5$ glasses up to 3% strain.

unloading back to zero stress). In each of these 4 physical conditions, we quantified the fraction of irreversible instabilities of the first instability in $M=100$ samples, as summarized in Fig. 4b. It is observed that the fraction of irreversible first instabilities is largest and close to unity for the high T_p samples (quick quench, poor annealing) under shear (small stress triaxiality) and that it decreases with both decreasing T_p (slower quench, better annealing) and increasing stress triaxiality (here, the dilatational limit). These results indicate that structural rearrangements under large stress triaxiality tend to be more reversible.

Next, we quantify the magnitude of structural rearrangements, whether reversible or irreversible, under shear and dilation. In Fig. 4c, we present the probability $p(s)$ of dimensionless stress drops s (see legend) during structural rearrangements under shear and dilation for quickly quenched (high T_p) samples up to 3% strain (smaller than ϵ_c). It is observed that stress drops under dilation are more than an order of magnitude smaller than those under shear. Hence, not only structural rearrangements under dilation tend to be more reversible but they are also significantly less intense, outweighing their larger rate observed in Fig. 2a and consistently with the significantly lower dilatational nonaffinity observed in Fig. 2a. Overall, these results explain the main observation in Fig. 3 that dilatational deformation up to large-scale cavitation is macroscopically reversible/elastic, largely independently of the glass thermal history. They do not, in themselves, explain its non-

linearity, i.e., the large dilatational hyperelasticity.

VII. First-principles zero-strain nonlinear elastic expansion

The large observed dilatational hyperelasticity is unusual. The most common and well-understood origin of hyperelasticity is entropic elasticity (‘rubber elasticity’) observed in soft solids such as rubber and polymers [61]. It typically emerges at large strains and its degree, i.e., the fractional change in the elastic modulus (either softening or stiffening) per unit strain, is usually rather mild. Stiffening hyperelasticity is also well-documented in underconstrained (sub-isostatic), disordered biopolymer networks and colloidal gels [62–65], which are qualitatively different from the dense glasses we studied. Our results suggest that dilatational hyperelasticity of glasses can be large, occur under small strains and its origin is energetic, not entropic. That is, they indicate that the observed large hyperelastic softening emerges from the nonlinearity of the interatomic interactions in the absence of significant dilatational irreversibility/plasticity.

This physical picture is translated into a strong theoretical prediction that the observed large hyperelastic softening under dilation quantitatively follows from the zero-strain ($\epsilon=0$) nonlinear elastic expansion

$$\frac{-P(\epsilon)}{dK_0} = \epsilon + \tilde{K}_2 \epsilon^2 + \mathcal{O}(\epsilon^3). \quad (1)$$

Here, K_0 is the bulk modulus as above, d is the spatial dimension (see *SI Appendix*) and $\tilde{K}_2 \equiv K_2/(dK_0)$ is the dimensionless second-order dilatational elastic constant. In the *SI Appendix*, we present first-principles expressions for K_0 and K_2 involving only the particle positions and interaction potential in the $\epsilon=0$ state. That is, we derive the nonlinear elastic expansion in Eq. (1) based only on the reference $\epsilon=0$ state, using a nonlinear response theory, involving no actual deformation [50].

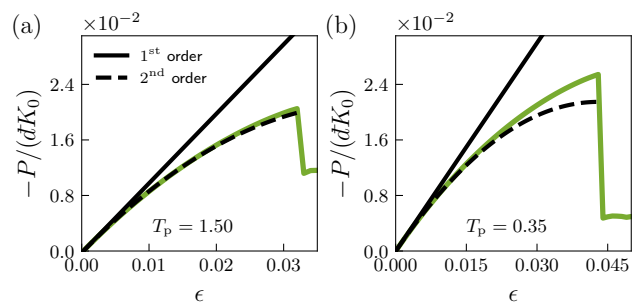


FIG. 5. (a-b) The same stress-strain curves as in Fig. 3a,c respectively, where the first-principles zero-strain expansion of Eq. (1) up to first order (solid line) and second order (dashed line) are superposed. See text for discussion.

The outcome is presented in Fig. 5, where the prediction in Eq. (1) is superposed on the dilatational stress-

strain curve of Fig. 3a,c, for the two widely different thermal histories, revealing excellent quantitative agreement up ϵ_c . We emphasize that this great agreement is achieved despite the fact that the loading process is punctuated by discontinuities associated with structural rearrangements/instabilities. The small deviations observed close to ϵ_c correspond to a third-order term in Eq. (1), not considered here. These results conclusively demonstrate the hyperelastic nature of dilatational glassy deformation approaching large-scale cavitation and its energetic origin.

VIII. Irreversible micro-cavities and the onset of large-scale cavitation

The predominantly hyperelastic dilatational deformation is truncated by a cavitation instability, upon which a large cavity spontaneously forms inside the glass, accompanied by a significant loss of load-bearing capacity. Unlike its shear counterpart, where shear-banding strongly depends on the glass thermal history, this dilatational phenomenology is qualitatively independent of it (quantitative difference do exist, see the different stress drops at different values of ϵ_c in Fig. 5). A comprehensive analysis and understanding of the irreversible cavitation instability go beyond the scope of this work. Yet, in light of the above results about the predominantly reversible nature of dilatational glassy deformation, it is important to pose the question of the emergence of irreversibility under dilation and the physically-relevant mesoscopic objects that mediate it.

To start addressing this question, it is natural to speculate that the large-scale cavity emerges from smaller-scale cavities that form under dilation and lose stability. To explore this possibility, we developed a micro-cavity detection algorithm (see *SI Appendix*) and apply it to a quickly quenched glass undergoing dilatational loading up to large-scale cavitation followed by unloading back to zero stress, and report the results in Fig. 6.

In Fig. 6a, we present snapshots of micro-cavities at different pre-cavitation loading strains $\epsilon \leq \epsilon_c^-$ (top row). It is observed that both the size and number of micro-cavities increase with ϵ , and their spatial distribution is homogeneous. The probability $p(V_{\text{cav}})$ of the micro-cavity volume V_{cav} at $\epsilon = 0$ and $\epsilon = \epsilon_c^-$, obtained over an ensemble of $M = 100$ samples, is presented in Fig. 6b, clearly demonstrating the significant increase in V_{cav} with ϵ . At $\epsilon = \epsilon_c^-$, the distribution features a power-law tail $p(V_{\text{cav}}) \sim (V_{\text{cav}})^{-3}$, apparently independently of the glass thermal history, see *SI Appendix*. Next, in Fig. 6a (bottom row, right), we present the cavities snapshot at $\epsilon = \epsilon_c^+$, which reveals a large, quasi-spherical cavity and a cloud of micro-cavities inhomogeneously surrounding it. This cavitation instability is the origin of the large stress drop observed in Figs. 1a,3a,5a.

The observed micro-cavities upon loading are not nec-

essarily irreversible. The physical irreversibility condition is expected to be related to the emergence of a curvature-dependent surface energy. While it is not discussed here, it is clear that once it is met for given micro-cavity, the latter will persist ('survive') upon unloading. A possibly related question concerns the critical nuclei for cavitation, i.e., whether a subset of the micro-cavity population at $\epsilon = \epsilon_c^-$ serves as a seed to large-scale cavity formation at $\epsilon = \epsilon_c^+$. This is indeed the case, and the relevant micro-cavity is marked on the $\epsilon = \epsilon_c^-$ snapshot. Then, snapshots of the micro-cavity population upon unloading are presented (bottom row), demonstrating that the very same micro-cavity survives unloading, i.e., it is irreversible (see zoom-in inset). Finally, $p(V_{\text{cav}})$ of unloaded samples is superposed on Fig. 6b, also revealing a signature of the irreversible micro-cavities at the tail of the distribution.

The scarcity of irreversible micro-cavities is a clear manifestation of the predominantly reversible/elastic nature of the pre-cavitation dilatational deformation of glasses. Yet, these objects are mesoscopic and do not exclude the emergence of atomistic irreversibility. To highlight this point, we superpose on the loading-unloading snapshots in Fig. 6a the magnitude of the particle-level nonaffine displacements, i.e., the magnitude of the displacement vector relative to the $\epsilon = 0$ configuration, once the global affine deformation is subtracted. It is observed that particle-level nonaffinity exists throughout the sample during the loading process, peaked prior to large-scale cavitation, and that part of it is irreversible, i.e., persists upon unloading.

IX. Universality across different glass formers

The results obtained for LJ glasses are expected to be representative of a broader class of glass formers. To explicitly demonstrate this, we studied a CuZr metallic glass using an EAM potential [66] and a silica glass using the SHIK potential [67], see *SI Appendix*. The resulting dilation loading-unloading curves are presented in Fig. 7a-b, following the same format of Fig. 3a. Macroscopic reversibility up to large-scale cavitation is observed in these two very different glass formers, significantly supporting the universality of our findings. Note that the large elastic hysteresis loop for silica is characterized by a two-step unloading process: an initial stage in which micro-cavities shrink with minute microscopic nonaffinity, followed by an abrupt increase in nonaffine motions of the glassy network.

The inset in Fig. 7a shows the loading tangent bulk modulus $K_t(\epsilon)$ up to cavitation of the CuZr glass, revealing a strong hyperelastic softening that is quantitatively similar to the corresponding behavior of the LJ glass in Fig. 1. The corresponding $K_t(\epsilon)$ of the silica glass is shown in the inset of Fig. 7b for small strains, below ϵ_c . We focus on small strains since the hyperelastic response in this range reveals stiffening, not softening, highlighting

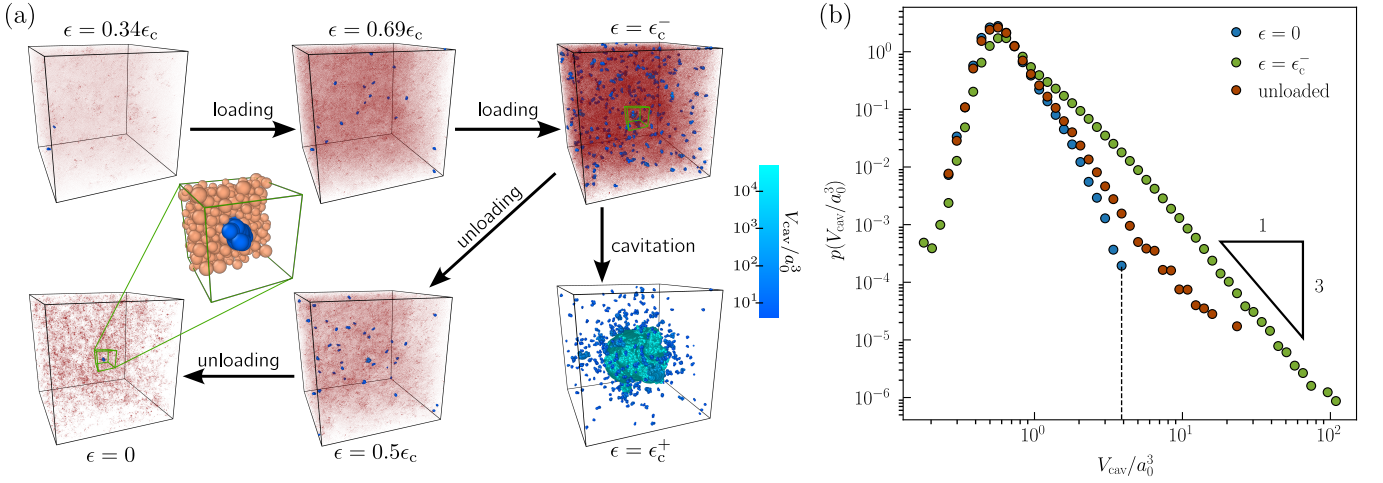


FIG. 6. (a) Spatial distributions of micro-cavities (labeled by volume V_{cav} , see right colorbar) and the magnitude of particle-level nonaffine displacements (in red) along the loading-unloading path of the dilated glass of Fig. 1a (see strain values ϵ and labeled arrows). The zoom-in inset shows an irreversible micro-cavity with its surrounding particles, featuring $V_{\text{cav}} = 11.3a_0^3$ with $a_0 \equiv [V(\epsilon=0)/N]^{1/3}$, also marked on the $\epsilon = \epsilon_c^-$ snapshot. See text for discussion. (b) $p(V_{\text{cav}}/a_0^3)$ at $\epsilon=0$, $\epsilon = \epsilon_c^-$ and the unloaded state (see legend), where the tail of the latter follows $\sim (V_{\text{cav}})^{-3}$. The vertical dashed line denotes the lower threshold for micro-cavity detection in panel (a).

that the degree of hyperelasticity and even its sign may depend on the class of glass formers. The subsequent softening observed in Fig. 7b at larger strains approaching cavitation, as well as the corresponding shear loading-unloading curves, are presented and discussed in the *SI Appendix*. Note that our dilatational silica results might be related to the experimental and simulational uniaxial tension results of [68, 69], though the basic question of the reversibility/irreversibility of the pre-failure deformation has not been addressed therein.

X. Summary and outlook

We demonstrated that the deformation and failure modes of glasses strongly depend on the stress triaxiality. Specifically, we showed that glasses under dilation, i.e., in the limit of large stress triaxiality, are predominantly elastic up to a large-scale cavitation instability — typically featuring significant hyperelasticity — largely independently of the glass thermal history. Dilated glasses feature nonaffinity and structural rearrangements related to their disordered nature, but these are either reversible (elastic) and/or of small magnitude, making little contribution to macroscopic plasticity. They also feature micro-cavities, a small fraction of which serve as critical nuclei for cavitation and may survive unloading. These findings are contrasted with the corresponding glass response under shear, i.e., in the limit of vanishing stress triaxiality.

Our findings are directly relevant for realistic deformation and failure of glasses, which generically take place under finite stress triaxiality levels, in many cases relatively high ones [26, 27]. They can be tested in experiments that are specifically designed to achieve high stress triaxiality levels. Our results also give rise to a plethora of questions and future investigation directions, briefly mentioned here. First, as already alluded to above, one needs to develop a better understanding of the physical conditions for the formation of irreversible micro-cavities and of the instability criterion associated with large-scale cavitation. Such a criterion may also shed light on the quantitatively different behavior revealed in silica. Moreover, one needs to characterize the spatiotemporal evolution of the cavity, which requires going beyond the AQS

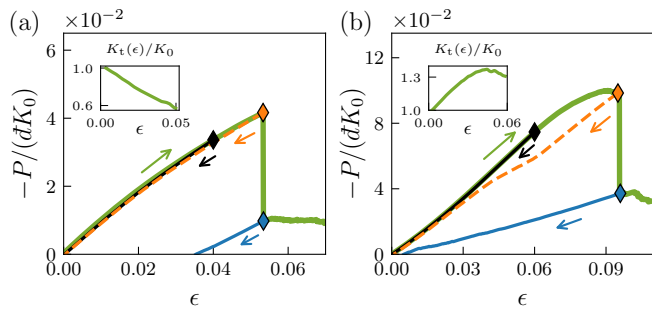


FIG. 7. (a) The dilation loading-unloading (up to ϵ_c) stress-strain curve for a computer CuZr metallic glass, see *SI Appendix*. (inset) The loading tangent modulus $K_t(\epsilon \leq \epsilon_c)$. (b) The same as panel (a), but for a computer model of silica glass, see *SI Appendix*. (inset) $K_t(\epsilon \leq 0.06 < \epsilon_c)$. See text for discussion.

limit, and to understand its size selection.

The natural next step would be to consider finite stress triaxiality levels, which are expected to give rise to stronger couplings between shear- and dilation-mediated deformation processes (e.g., there exists evidence that shear softening can facilitate the formation of microcavities [22, 39, 70, 71]), though the roles of dilatational hyperelasticity — discussed in this work — in these processes are entirely unexplored. The emerging physical insights should be incorporated into various coarse-grained theoretical efforts, such as elasto-plastic models [72–74] and internal-variable based continuum constitutive rela-

tions [34, 75, 76].

ACKNOWLEDGMENTS

E.B. acknowledges support from the Israel Science Foundation (ISF Grant No. 403/24) and the Harold Perlman Family.

(*) The *SI Appendix* will be added.

-
- [1] S. Timoshenko, *History of strength of materials: with a brief account of the history of theory of elasticity and theory of structures* (Courier Corporation, 1983).
- [2] A. A. Benzerga, J.-B. Leblond, A. Needleman, and V. Tvergaard, Ductile failure modeling, *Int. J. Fract.* **201**, 29 (2016).
- [3] F. A. McClintock, A criterion for ductile fracture by the growth of holes, *Journal of Applied Mechanics* **35**, 363 (1968).
- [4] J. R. Rice and D. M. Tracey, On the ductile enlargement of voids in triaxial stress fields, *Journal of the Mechanics and Physics of Solids* **17**, 201 (1969).
- [5] J. Lemaitre, *A course on damage mechanics* (Springer science & business media, 2012).
- [6] J. Lemaitre, A continuous damage mechanics model for ductile fracture, *Journal of Engineering Materials and Technology* **107**, 83 (1985).
- [7] J. Lemaitre, How to use damage mechanics, *Nuclear engineering and design* **80**, 233 (1984).
- [8] J. Lemaitre, Local approach of fracture, *Engineering Fracture Mechanics* **25**, 523 (1986).
- [9] J. L. Chaboche, Continuum damage mechanics: Part i-general concepts, *Journal of Applied Mechanics* **55**, 59 (1988).
- [10] J. L. Chaboche, Continuum damage mechanics: Part ii-damage growth, crack initiation, and crack growth, *Journal of Applied Mechanics* **55**, 65 (1988).
- [11] N. Bonora, A nonlinear cdm model for ductile failure, *Engineering fracture mechanics* **58**, 11 (1997).
- [12] T.-J. Wang, Unified cdm model and local criterion for ductile fracture-ii. ductile fracture local criterion based on the cdm model, *Engineering Fracture Mechanics* **42**, 185 (1992).
- [13] S. Chandrakanth and P. Pandey, An isotropic damage model for ductile material, *Engineering fracture mechanics* **50**, 457 (1995).
- [14] G. La Rosa, G. Mirone, and A. Risitano, Effect of stress triaxiality corrected plastic flow on ductile damage evolution in the framework of continuum damage mechanics, *Engineering Fracture Mechanics* **68**, 417 (2001).
- [15] A. L. Gurson, Continuum theory of ductile rupture by void nucleation and growth: Part i-yield criteria and flow rules for porous ductile media, *Journal of Engineering Materials and Technology* **99**, 2 (1977).
- [16] V. Tvergaard and A. Needleman, Analysis of the cup-cone fracture in a round tensile bar, *Acta metallurgica* **32**, 157 (1984).
- [17] A. Needleman and V. Tvergaard, An analysis of ductile rupture in notched bars, *Journal of the Mechanics and Physics of Solids* **32**, 461 (1984).
- [18] V. Tvergaard and J. W. Hutchinson, Two mechanisms of ductile fracture: void by void growth versus multiple void interaction, *International Journal of Solids and Structures* **39**, 3581 (2002).
- [19] Q. An, G. Garrett, K. Samwer, Y. Liu, S. V. Zybin, S.-N. Luo, M. D. Demetriou, W. L. Johnson, and W. A. Goddard III, Atomistic characterization of stochastic cavitation of a binary metallic liquid under negative pressure, *The Journal of Physical Chemistry Letters* **2**, 1320 (2011).
- [20] P. Guan, S. Lu, M. J. Spector, P. K. Valavala, and M. L. Falk, Cavitation in amorphous solids, *Phys. Rev. Lett.* **110**, 185502 (2013).
- [21] X. Lei, C. Li, X. Shi, X. Xu, and Y. Wei, Notch strengthening or weakening governed by transition of shear failure to normal mode fracture, *Scientific reports* **5**, 10537 (2015).
- [22] L. Meng, Y. Zhang, X. Tang, and X. Yao, Stress-induced failure transition in metallic glasses, *Int. J. Plast.* **183**, 104152 (2024).
- [23] B. Lawn, *Fracture of Brittle Solids* (Cambridge University Press).
- [24] J. Fineberg and M. Marder, Instability in dynamic fracture, *Physics Reports* **313**, 1 (1999).
- [25] S. A. Atroshenko, N. Morozov, W. Zheng, Y. Huang, Y. V. Sudenkov, N. Naumova, and J. Shen, Deformation behaviors of a tizrn cube bulk metallic glass under shock loading, *J. Alloy. Compd.* **505**, 501 (2010).
- [26] T. C. Hufnagel, U. K. Vempati, and J. D. Almer, Crack-tip strain field mapping and the toughness of metallic glasses, *PLoS One* **8**, e83289 (2013).
- [27] X. W. Gu, M. Jafary-Zadeh, D. Z. Chen, Z. Wu, Y.-W. Zhang, D. J. Srolovitz, and J. R. Greer, Mechanisms of failure in nanoscale metallic glass, *Nano letters* **14**, 5858 (2014).
- [28] J. Pan, H. Zhou, Z. Wang, Y. Li, and H. Gao, Origin of anomalous inverse notch effect in bulk metallic glasses, *J. Mech. Phys. Solids* **84**, 85 (2015).
- [29] J. Pan, Y. Wang, and Y. Li, Ductile fracture in notched bulk metallic glasses, *Acta Materialia* **136**, 126 (2017).
- [30] J. Rong, P. Zhu, and Y. Xu, Molecular dynamics simulation of spallation of metallic glasses under ultra-high

- strain rates, *Mater. Today Commun.* **33**, 104597 (2022).
- [31] M. Cheng, Y. Zhang, L. Meng, and X. Yao, The atomistic mechanism of notch sensitivity on the deformation mode in metallic glasses, *Journal of Applied Physics* **131**, 225108 (2022).
- [32] M. Falk, Molecular dynamics study of ductile and brittle fracture in model noncrystalline solids, *Phys. Rev. B* **60**, 7062 (1999).
- [33] P. Murali, T. Guo, Y. Zhang, R. Narasimhan, Y. Li, and H. Gao, Atomic scale fluctuations govern brittle fracture and cavitation behavior in metallic glasses, *Phys. Rev. Lett.* **107**, 215501 (2011).
- [34] C. H. Rycroft and E. Bouchbinder, Fracture toughness of metallic glasses: Annealing-induced embrittlement, *Phys. Rev. Lett.* **109**, 194301 (2012).
- [35] I. Singh, R. Narasimhan, and U. Ramamurty, Cavitation-induced fracture causes nanocorrugations in brittle metallic glasses, *Phys. Rev. Lett.* **117**, 044302 (2016).
- [36] L.-Q. Shen, J.-H. Yu, X.-C. Tang, B.-A. Sun, Y.-H. Liu, H.-Y. Bai, and W.-H. Wang, Observation of cavitation governing fracture in glasses, *Science Advances* **7**, eabf7293 (2021).
- [37] X. Tang, L. Shen, H. Zhang, W. Li, and W. Wang, Crack tip cavitation in metallic glasses, *J. Non-Cryst. Solids* **592**, 121762 (2022).
- [38] B. Sun and W. Wang, The fracture of bulk metallic glasses, *Prog. Mater. Sci.* **74**, 211 (2015).
- [39] D. Richard, E. T. Lund, J. Schroers, and E. Bouchbinder, Bridging necking and shear-banding mediated tensile failure in glasses, *Phys. Rev. Mater.* **7**, L032601 (2023).
- [40] U. A. Dattani, S. Karmakar, and P. Chaudhuri, Universal mechanical instabilities in the energy landscape of amorphous solids: Evidence from athermal quasistatic expansion, *Phys. Rev. E* **106**, 055004 (2022).
- [41] A. Moriel, D. Richard, E. Lerner, and E. Bouchbinder, Elementary processes in dilatational plasticity of glasses, *Phys. Rev. Research* **6**, 023167 (2024).
- [42] S. Bonfanti, R. Guerra, C. Mondal, I. Procaccia, and S. Zapperi, Elementary plastic events in amorphous silica, *Phys. Rev. E* **100**, 060602 (2019).
- [43] A. S. Argon, Plastic deformation in metallic glasses, *Acta Metallurgica* **27**, 47 (1979).
- [44] M. L. Falk and J. S. Langer, Dynamics of viscoplastic deformation in amorphous solids, *Physical Review E* **57**, 7192 (1998).
- [45] P. M. Anderson, J. P. Hirth, and J. Lothe, *Theory of dislocations* (Cambridge University Press, 2017).
- [46] K. González-López, M. Shivam, Y. Zheng, M. P. Ciaramarra, and E. Lerner, Mechanical disorder of sticky-sphere glasses. I. effect of attractive interactions, *Phys. Rev. E* **103**, 022605 (2021).
- [47] A. Ninarello, L. Berthier, and D. Coslovich, Models and algorithms for the next generation of glass transition studies, *Phys. Rev. X* **7**, 021039 (2017).
- [48] C. Maloney and A. Lemaitre, Subextensive scaling in the athermal, quasistatic limit of amorphous matter in plastic shear flow, *Phys. Rev. Lett.* **93**, 016001 (2004).
- [49] C. E. Maloney and A. Lemaitre, Amorphous systems in athermal, quasistatic shear, *Physical Review E* **74**, 016118 (2006).
- [50] S. Karmakar, E. Lerner, and I. Procaccia, Athermal nonlinear elastic constants of amorphous solids, *Phys. Rev. E* **82**, 026105 (2010).
- [51] B. Xu, M. Falk, J. Li, and L. Kong, Strain-dependent activation energy of shear transformation in metallic glasses, *Phys. Rev. B* **95**, 144201 (2017).
- [52] Y. Jin, P. Urbani, F. Zamponi, and H. Yoshino, A stability-reversibility map unifies elasticity, plasticity, yielding, and jamming in hard sphere glasses, *Science advances* **4**, eaat6387 (2018).
- [53] G. Kapteijns, W. Ji, C. Brito, M. Wyart, and E. Lerner, Fast generation of ultrastable computer glasses by minimization of an augmented potential energy, *Physical Review E* **99**, 012106 (2019).
- [54] D. Richard, M. Ozawa, S. Patinet, E. Stanifer, B. Shang, S. A. Ridout, B. Xu, G. Zhang, P. Morse, J.-L. Barrat, *et al.*, Predicting plasticity in disordered solids from structural indicators, *Physical Review Materials* **4**, 113609 (2020).
- [55] A. Heuer, Exploring the potential energy landscape of glass-forming systems: from inherent structures via metabasins to macroscopic transport, *J. Condens. Matter Phys.* **20**, 373101 (2008).
- [56] S. Singh, M. D. Ediger, and J. J. De Pablo, Ultrastable glasses from in silico vapour deposition, *Nat Mater.* **12**, 139 (2013).
- [57] A. D. Parmar, M. Ozawa, and L. Berthier, Ultrastable metallic glasses in silico, *Phys. Rev. Lett.* **125**, 085505 (2020).
- [58] F. Varnik, L. Bocquet, J.-L. Barrat, and L. Berthier, Shear localization in a model glass, *Phys. Rev. Lett.* **90**, 095702 (2003).
- [59] Y. Shi and M. L. Falk, Strain localization and percolation of stable structure in amorphous solids, *Phys. Rev. Lett.* **95**, 095502 (2005).
- [60] M. Ozawa, L. Berthier, G. Biroli, A. Rosso, and G. Tarjus, Random critical point separates brittle and ductile yielding transitions in amorphous materials, *Proc. Natl. Acad. Sci. U.S.A.* **115**, 6656 (2018).
- [61] L. G. Treloar, *The physics of rubber elasticity* (Oxford University Press, 1975).
- [62] C. Storm, J. J. Pastore, F. C. MacKintosh, T. C. Lubensky, and P. A. Janmey, Nonlinear elasticity in biological gels, *Nature* **435**, 191 (2005).
- [63] G. de Oliveira Reis, T. Gibaud, B. Saint-Michel, S. Manneville, M. Leocmach, L. Vaysse, F. Bonfils, C. Sanchez, and P. Menu, Irreversible hardening of a colloidal gel under shear: The smart response of natural rubber latex gels, *J. Colloid Interface Sci.* **539**, 287 (2019).
- [64] E. Lerner and E. Bouchbinder, Scaling theory of critical strain-stiffening in disordered elastic networks, *Extreme Mech. Lett.* **65**, 102104 (2023).
- [65] Z. Zhang, E. Bouchbinder, and E. Lerner, The strain-stiffening critical exponents in polymer networks and their universality, *The Journal of Chemical Physics* **163**, 111102 (2025).
- [66] M. Mendelev, Y. Sun, F. Zhang, C.-Z. Wang, and K.-M. Ho, Development of a semi-empirical potential suitable for molecular dynamics simulation of vitrification in cu-zr alloys, *J. Chem. Phys.* **151**, 214502 (2019).
- [67] S. Sundararaman, L. Huang, S. Ispas, and W. Kob, New interaction potentials for borate glasses with mixed network formers, *J. Chem. Phys.* **152**, 104501 (2020).
- [68] P. K. Gupta and C. R. Kurkjian, Intrinsic failure and non-linear elastic behavior of glasses, *J. Non-Cryst. Solids* **351**, 2324 (2005).
- [69] Z. Zhang, S. Ispas, and W. Kob, Origin of the non-linear elastic behavior of silicate glasses, *Acta Materialia* **231**,

- 117855 (2022).
- [70] R. Maass, P. Birckigt, C. Borchers, K. Samwer, and C. A. Volkert, Long range stress fields and cavitation along a shear band in a metallic glass: The local origin of fracture, *Acta Materialia* **98**, 94 (2015).
- [71] J. Luo and Y. Shi, Tensile fracture of metallic glasses via shear band cavitation, *Acta Materialia* **82**, 483 (2015).
- [72] E. R. Homer and C. A. Schuh, Mesoscale modeling of amorphous metals by shear transformation zone dynamics, *Acta Materialia* **57**, 2823 (2009).
- [73] B. Kondori, A. A. Benzerga, and A. Needleman, Discrete shear transformation zone plasticity, *Extreme Mech. Lett.* **9**, 21 (2016).
- [74] A. Nicolas, E. E. Ferrero, K. Martens, and J.-L. Barrat, Deformation and flow of amorphous solids: Insights from elastoplastic models, *Rev. Mod. Phys.* **90**, 045006 (2018).
- [75] D. Henann and L. Anand, A constitutive theory for the mechanical response of amorphous metals at high temperatures spanning the glass transition temperature: Application to microscale thermoplastic forming, *Acta Materialia* **56**, 3290 (2008).
- [76] M. L. Falk and J. S. Langer, Deformation and failure of amorphous, solidlike materials, *Annu. Rev. Condens. Matter Phys.* **2**, 353 (2011).